Article, Published Version

Dao, Hoang Tung; Hofland, Bas; Suzuki, Tomohiro; Stive, Marcel J. F.; Mai, Tri; Tuan, Le Xuan

Numerical and Small-scale Physical Modelling of Wave Transmission by Wooden Fences

Journal of Coastal and Hydraulic Structures

Zur Verfügung gestellt in Kooperation mit/Provided in Cooperation with:
TU Delft

Verfügbar unter/Available at: https://hdl.handle.net/20.500.11970/108215

Vorgeschlagene Zitierweise/Suggested citation:
Dao, Hoang Tung; Hofland, Bas; Suzuki, Tomohiro; Stive, Marcel J. F.; Mai, Tri; Tuan, Le Xuan (2021): Numerical and Small-scale Physical Modelling of Wave Transmission by Wooden Fences. In: Journal of Coastal and Hydraulic Structures 1.

JOURNAL OF COASTAL AND HYDRAULIC STRUCTURES

Vol. 1, 2021, 4

Numerical and Small-scale Physical Modelling of Wave Transmission by Wooden Fences

Hoang Tung Dao [1], Bas Hofland [2], Tomohiro Suzuki [3], Marcel J. F. Stive [4], Tri Mai [5] and Le Xuan Tuan [6]

Abstract

Mangrove forests, that often act as natural coastal defences, enormously suffered due to ongoing climate change and human disturbances. Thus, it is necessary to have a countermeasure to mitigate the loss of mangroves. Wooden fences are becoming a viable nature-based solution to protect vulnerable replanted mangrove forests. However, the wooden fence's hydraulic characteristics are not yet fully understood due to the complication of branches arrangement. In the present study, a small-scale fence was tested in a wave flume to investigate the wave damping by wooden fences. The inner branches of the fence had the same inhomogeneous arrangement as used in earlier flow-resistance experiments. The physical model results indicate that the wooden fence is highly effective on wave transmission and that the effectiveness in wave reduction depends on the relative fence thickness, B/H_I. To understand the scale effect on wave transmission further, the numerical model SWASH was used with the laboratory wave data. By applying the prior experiments' drag coefficient on steady flow, the uncalibrated numerical model gave a good agreement with the wave model results, with a root-mean-square error for the total transmitted wave heights of 4.7%. After validation, potential scale effects for small scale tests were determined from scaling simulations at both full scales and the applied 1:5 model scale. These simulations were performed for a fence porosity of 0.81, and different fence thicknesses to understand scale effects between model- and full-scale. Both wave reflection and transmission at model-scale are about 5% higher than full-scale results due to the increased drag coefficient and viscous effects. The effects of fence thickness and porosity were the same in large and small scale, and much larger than the error due to scale effects. Hence testing fence efficiency at physical small scale is regarded as a useful tool, together with numerical modelling.

Keywords

Nature-based solution, brushwood fence, wave damping, numerical modelling, SWASH, physical modelling, Mekong Delta

[1] h.t.dao@tudelft.nl, Faculty of Civil Engineering and Geosciences, Delft University of Technology, Delft, The Netherlands.
[2] b.hofland@tudelft.nl, Faculty of Civil Engineering and Geosciences, Delft University of Technology, Delft, The Netherlands.
[3] tomohiro.suzuki@mow.vlaanderen.be, Flanders Hydraulics Research, Antwerp, Belgium
[4] m.j.f.stive@tudelft.nl, Faculty of Civil Engineering and Geosciences, Delft University of Technology, Delft, The Netherlands.
[5] trimc@nuce.edu.vn, Faculty of Coastal and Offshore Engineering, National University of Civil Engineering, Hanoi, Vietnam
[6] tuan.mangrove@gmail.com, Faculty of Biology, University of Science, Vietnam National University, Hanoi, Vietnam

This paper was submitted on 2 March 2021.
It was accepted after double-blind review on 30 April 2021 and published online on 24 June 2021.

DOI: https://doi.org/10.48438/jchs.2021.0004

Cite as: "Dao, T. H., Hofland, B., Suzuki, T., Stive, M. J. F., Mai, T., & Tuan, L. X. (2021). Numerical and small-scale physical modelling of wave transmission by wooden fences. Journal of Coastal and Hydraulic Structures, 1. https://doi.org/10.48438/jchs.2021.0004."

1 Introduction

Mangrove forests play a significant role as coastal defences by dissipating wave and current energies and opening an opportunity to protect the shore and expand the coast (Del Valle et al. 2020). However, mangrove forests have been facing severe degradation due to ongoing climate change and human disturbances. Hard structures, such as sea dikes and revetments, are usually used to protect the coastlines from erosion under design conditions but ultimately may cause mangrove squeeze (Phan et al. 2014). To restore mangroves nature-based solutions, such as wooden fences, might well be a better choice that can be installed temporarily in front of newly replanted mangrove forests. In Figure 1, a wooden fence is shown that was constructed from mainly natural materials. The assembly consists of two (Figure 1a) to three (Figure 1b) lines of vertical bamboo poles, with forwarding-oriented poles that cover the horizontal branches (brushwood bundles) of the inner parts (Albers et al. 2013; Anh et al. 2018; Van Cuong et al. 2015; Gijón Mancheño et al. 2017; Schmitt et al. 2013; Schmitt and Albers 2014; Thieu Quang and Mai Trong 2020).

Figure 1: Type of bamboo fences in the Mekong Delta. Courtesy Hoang Tung Dao, 2016 (a) and Le Xuan Tuan, 2020 (b).

Studies of wave reduction due to brushwood fences with a similar structure have been carried out in physical and numerical models. Sayah and Schleiss (2006) investigated wave-fence interaction in a physical scale model, which pointed out the dominant role of wave steepness and porosity and concluded that wave reduction depended on dominant wave steepness in response to the density of the structure. Mai (1999) also investigated wave transmission through prototype-scale brushwood fences, which appeared to be strongly dependent on the wave period. Interestingly, both studies suggested that the main parameter influenced wave transmission was the relative freeboard (R_C/H_I), with R_C is the freeboard defining the difference of fence crest and water surface. Recently, Thieu Quang and Mai Trong (2020) numerically examined the existing field data of wave damping due to bamboo fences in the Lower Mekong Delta (Albers et al. 2013; Schmitt et al. 2013). With numerical results, an empirical formulation of wave transmission by wooden fences was consequently derived from field data, a function of the relative freeboard, fence thickness and porosity. Dao et al. (2018) numerically studied wave reduction due to a wooden fence as vertical cylinders to mimic the fence. This study suggested that the wave damping increases with the increase of both wave nonlinearity, as indicated by the Ursell number, and the thickness of wooden fences. Moreover, field experiments of wave reduction due to wooden fences were carried out along Mekong Delta coasts which wave and current energies were significantly reduced by wooden fences (Albers et al. 2013; Van Cuong et al. 2015; Schmitt et al. 2013). The above studies only point out the relationship between wave transmission and the geometrical parameter of wooden fences, i.e., freeboard and thickness.

To estimate wave reduction by an array of cylinders, most often used to mimic a vegetation area, both energy-balance (phase-averaged) models and the momentum-balance (phase-resolved) models are applied. These models use the effect of drag forces exerted on rigid cylinders, as expressed by the Morison equations (Morison et al. 1950), to determine the wave energy loss due to cylinders. Due to the increased simulated resolution, the phase-resolved models consume more computation time than the phase-averaged models. Dalrymple et al. (1984) modified the energy-conservation models by adding the effect of wave breaking and irregular waves (Mendez and Losada 2004) that was further developed by

including wave dissipation with layer schematization (Suzuki et al. 2012) and wave dissipation in the vertical direction on horizontal cylinders that is absent for vertical cylinders (Suzuki et al. 2019). In the newest model, the process of wave reduction due to an array of cylinders can be quantified in detail by the characteristics of the cylinder array, i.e., diameter (D_v, m), density (N_v, cylinders/m^2) and the bulk drag coefficient ($\overline{C_D}$).

Additionally, the description of flow and wave resistance of wooden fences and vegetation are comparable, as both are essentially caused by the drag forces on an array of cylinders. From this perspective, the bulk drag coefficient, therefore, is an important parameter to characterize the flow and wave resistance by vegetation. The bulk coefficient was generally investigated by the physical model, which used only for vertical cylinders mimicking vegetated areas (Anderson and Smith 2014; Chen et al. 2018; Hu et al. 2014; Ozeren et al. 2013; Tanino and Nepf 2008). Because of the effects of shielding and blockage around vertical cylinders with a high density, the bulk drag coefficient inside an area of cylinders is often higher than its value for a single-cylinder in an open flow (Hu et al. 2014; Ozeren et al. 2013). However, for the complex orientation of vegetation in the field where mangrove roots have an inhomogeneous orientation, i.e., schematically vertical, and horizontal orientations, the bulk drag coefficient is usually underestimated. Dao et al. (2020) carried out a series of experiments to investigate bamboo fences' flow resistance by assessing the bulk drag forces under stationary flow. The bulk drag coefficient of inhomogeneous and staggered arrangements was obtained in both a model- and full-scale experiment, strongly influenced by the porosity, random arrangement, and Reynolds number.

In this study, a 2D physical model was built to generate a validation data set for wave damping due to wooden fences in model-scale. In this physical model, the brushwood branches with an inhomogeneous arrangement were used to mimic the irregular configuration applied in the real wooden fences (Figure 1). Next, this 2D model was reproduced in a numerical model to validate the momentum balance model which was applied in the time-domain wave-model SWASH (Simulation Wave till Shore) (Zijlema et al. 2011). SWASH is a general-purpose numerical model to simulate non-hydrostatic and free-surface flow phenomena in the coastal water (Phan et al. 2019; Reis et al. 2020). The bulk drag coefficient is typically used as a calibration parameter such that a pure validation is not possible. Therefore, the bulk drag coefficient, separately obtained in another experimental set-up for model- and full-scale fences by Dao et al. (2020), was applied to run the numerical model for the validation (Table 1). In the next step, the bulk drag coefficient for full-scale fences, that was also obtained in Dao et al. (2020), was applied to repeat the calculation at full-scale. Based on the bulk drag coefficient results in the full-scale SWASH model, the scale effects of wave damping due to wooden fences could be estimated while, the applied model set-up was still validated by empirical observation.

This study is organized as follows. In section 2, the methodology is presented in several subsections, describing the interaction processes between wave and wooden fence, the scale consideration, the physical and numerical model descriptions. The validation of the numerical model is presented, and the scaling simulations results are illustrated in section 3. The discussion is presented in Section 4. Finally, the conclusions are provided in section 5.

2 Methods

In this section, first, the wave-fence interactions are introduced, including wave reflection, wave dissipation, and wave transmission processes. Next, several scaling considerations are presented to choose the scaling factor for scaling wooden fence characteristics and wave conditions. Next, the physical model of wave-fence interactions of the model-scale is described. Finally, the numerical model reconstructs the physical model used to validate the physical data and its uses for scaling the computations.

2.1 Wave-Fence interaction

Three main processes often characterize the interaction between wave and wooden fences, i.e., wave reflection in front and wave dissipation inside, resulting in wave transmission behind the wooden fence. In some conditions overtopping and breaking waves influence these processes, depending on water depth, inhomogeneous structures, and incoming wave height. The common expression for wave-fence interactions that was proposed for wave-porous structures by Thornton and Calhoun (1972) can be described as

$$K_R^2 + K_D^2 + K_T^2 = 1 \quad (1)$$

where K_D is the dissipation coefficients; K_R and K_T are the reflection and transmission coefficients, respectively, which is indicated as:

$$K_R = \frac{H_R}{H_I} \quad (2)$$

$$K_T = \frac{H_T}{H_I} \quad (3)$$

where H_I, H_R and H_T correspond to the incident, reflected, and transmitted (significant) wave heights. The definition of these wave heights is indicated further in the Physical model section.

The degree of dissipation is influenced by the fill material inside the structure. As mentioned, a wooden fence is mainly constructed by bamboo branches which create the dissipation caused by drag and friction. The drag and friction by cylinders are strongly dependent on the flow regime around the cylinders. The hydrodynamic quantities of oscillatory flow in a porous medium can be described by both the Keulegan-Carpenter number (KC number) with $KC = uT/D$ and Reynolds number (Re) with $Re = uD/\nu$ where T is the wave period, ν (m^2/s) is the kinematic viscosity, u (m/s) is the flow velocity for a steady flow or orbital velocity for an oscillation flow, and D (m) is cylinder diameter. The relationship between the drag coefficient for a single cylinder (C_D) and KC number has been reported by Keulegan and Carpenter (1958) for wave-cylinder interaction and by Mendez and Losada (2004), Ozeren et al. (2013), and Chen et al. (2018) for wave-vegetation interaction. The relationship between bulk coefficient $\overline{C_D}$ and Reynold numbers for wave-vegetation interaction has been suggested by, amongst others, Hu et al. (2014). The $\overline{C_D}$ values were even more complicated due to the inhomogeneous arrangement as well as to the high density for wooden fences, which were discussed for flow-fence interaction in Dao et al. (2020). Dao et al. (2020) tested the different arrangements of the inner parts (i.e., the inhomogeneous and staggered configuration) in 1:5 model-scale (D_m) and full-scale diameters (D_m). It is noted that subscript "m" and "p" are denoted for respectively small and full scales. The bulk drag coefficient with the formulation $Re_n - \overline{C_D}$ is shown in Table 1.

Table 1: Drag coefficient formulas (Dao et al. 2020).

No.	Formulas	Arrangement	Porosity (n)	Diameter (mm)	Filter velocity (m/s)	Scale
1	$\overline{C_{D,m1}} = 3.87 + \left(\frac{177.2}{Re_n}\right)^{1.23}$	Inhomogeneous	0.89	4.0	0.0 – 0.4	1:5
2	$\overline{C_{D,m2}} = 1.99 + \left(\frac{326}{Re_n}\right)^{0.65}$	Staggered	0.81	4.0	0.0 – 0.4	1:5
3	$\overline{C_{D,p1}} = 1.98 + \left(\frac{586}{Re_n}\right)^{1.39}$	Staggered	0.81	20.0	0.0 – 0.4	Full

2.2 Scaling considerations

A down-scaled model often represents the real-world prototype used to indicate the technical and economic solutions of hydraulic engineering problems (Novák and Čábelka 1981). In hydraulic engineering, Froude scaling is often used to up-scale physical model results (Heller 2011). The scale models reproduce aspects like non-linear waveforms and multi-scale turbulence phenomena rather well if the scale model is not too small. However, as a result of the different scales, scale effects occur due to a lack of ability to keep each relevant force ratio constant between small and full-scale models (Heller 2011; Hughes 1993). Generally, the scale effect for a specific phenomenon increases with the length scales which is the ratio of characteristic length of real-world to model length. Thus, the scale effect increases with the decreasing size of the model. In numerical models, the effects that lead to scale effects at the small scale can be switched on or off, for example, the effects of kinematic viscosity that increase the drag on cylinders, bed friction, or surface tension.

To scale wave conditions in this study, the Froude time scale (Hughes 1993) is applied as $N_T = \sqrt{N_L}$, where $N_L = D_p/D_m$ is the length scale. As mentioned, the inner parts of the wooden fence were tested for flow resistances with two main arrangements (Dao et al. 2020): (1) the inhomogeneous mimicking the field arrangement for model scale, and (2) the staggered arrangement for both model scale and full scale. The tested diameters of the horizontal branches were chosen

as 4.0 mm (D_m) and 20.0 mm (D_m) for the model- and full-scale fences, respectively. As a result, the length and time scales are N_L = 5.0 and N_T = 2.2 , respectively.

The hydraulic test conditions are chosen to resemble those of the north side of the Mekong Delta coast. For the wave conditions, at a distance of 100 km from the shore of the Mekong Delta coast, the water depth reaches nearly 30 m, where the highest significant wave height and wave period in a return period of 100 years are about 10.5 m and 11.5 seconds, respectively (Hoang and Nguyen 2006). Near the shore, the coast is a gently sloping foreshore with a slope from 1:500 to 1:1000 (Thieu Quang and Mai Trong 2020). The water depth for these slopes is about 2.0 m (Anh et al. 2018; Thieu Quang and Mai Trong 2020) under the semi-diurnal tide with an amplitude of 2.5 m to 3.8 m (Gagliano and McIntire 1968; Nguyen et al. 2000; Ta et al. 2002; Wolanski et al. 1996). A combination of the low water depth and the gently sloping foreshore can generate a strong environmental dissipation for waves. Thus, the primary wind waves will quickly lose their energy in the transmission process. As a result, wave heights, before reaching the foreshore, were reported below 0.8 m and wave periods ranged from 4.0 to 7.5 seconds at a water depth of nearly 2.0 m (Thieu Quang and Mai Trong 2020). Moreover, the characteristics of wooden fences in the Mekong Delta coast were reported in Schmitt et al. (2013), Albers et al. (2013), Ngo et al. (2018) and Thieu Quang and Mai Trong (2020). The typical characteristics of the fences include a maximum thickness of 1.2 m, and a height of 1.6 m at a water depth of 2.0 m during high tide and under submerged conditions. In this study, characteristics of wooden fences and wave conditions were scaled down based on the maximum values, and they are presented in Table 2.

Table 2: Characteristics of wave conditions and wooden fences in full and 1:5 model-scale.

Maximum value	Full scale	Model scale (1:5)
Fence height (m)	1.6	0.32
Fence thickness (m)	1.2	0.24
Water depth (m)	2.0	0.40
Significant wave height (m)	1.0	0.2
Peak wave period (s)	7.5	3.4

2.3 Physical model

In the Mekong Delta, the very gentle foreshore slopes (order 1/10,000) create a significantly attenuated environment for waves (Phan et al. 2014) before interacting with wooden fences. The gentle slopes generally cause an increase in the longwave energies after dissipating mostly short wave energies so that these energies are of the same order-of-magnitude and their negative correlation changes into a positive one at the entrance of the shallow zone to the brushwood fence location (Roelvink and Stive 1989). It is nearly impossible to scale such extremely gentle slopes of Mekong Delta in a wave flume, such as the wave flume in Delft University of Technology. Therefore, the generation of free-long waves from forcing a wave train with bound-long waves to break at a steep slope (Buckley et al. 2015; Tsai et al. 2005) is applied to mimic the slope needed.

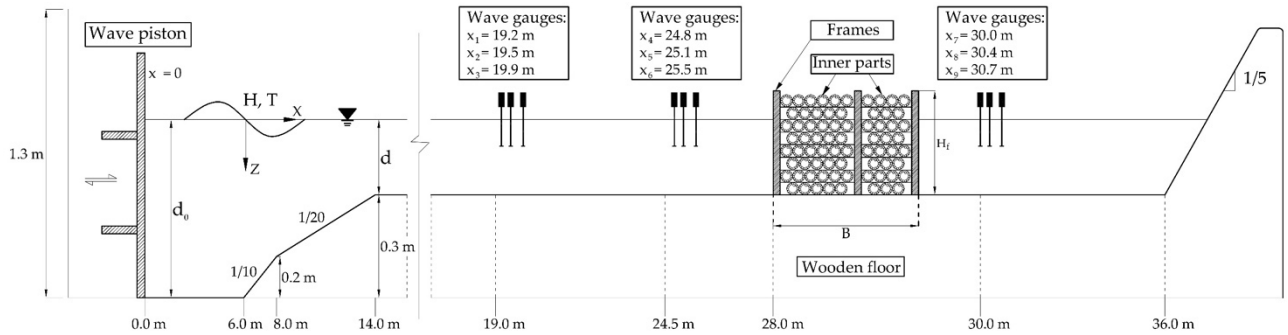

Figure 2: Schematization profile used in physical and SWASH model.

Physical tests of wave interaction with wooden fences were conducted in the wave flume in the Hydraulic Engineering Laboratory at Delft University of Technology. The wave flume measures 38 m x 0.8 m x 1.0 m. The applied set-up is shown in Figure 2 and represents the Mekong Delta cross-shore profile in a schematic and truncated fashion. The deep and shallow zone are connected by a composite slope of 1:10 and 1:20, where the offshore waves adapt to the shallow part by shoaling and breaking. At the left side of the flume, the wave generator (wave piston) is equipped with both Active Reflection Compensation (ARC) and second-order wave steering. At the downstream side, an impermeable smooth dike with a slope of 1:5 was installed to mimic the real dike along the foreshore of the Mekong Delta coast. In the shallow zone, nine Wave-Gauges (WGs) were installed in front and behind the wooden fence at x = 28.0 m (Figure 2).

Figure 3: Model wooden fences in the physical tests.

The model wooden fence (Figure 3) included a frame and the inner parts. The inner parts mimicked the configuration of a fence in the field, as shown in Figure 1. According to Schmitt and Albers (2014), three rows of vertical bamboo piles created the largest thickness (B = 1.2 m, see Table 2) and two layers of piles for smaller thicknesses. The increase of vertical rows increases the structural stability for larger thicknesses. The same structure was also successfully used in another place along the Mekong Delta coast, as corroborated by Ngo et al. (2018). In the present physical test, the construction with three vertical rows was applied for the largest thickness. The top-view of this fence set-up is presented in Figure 4b. Three thicknesses were used in this physical test, including B = 0.28 m; 0.40 m; and 0.66 m, while only one fence height, H_f = 0.30 m, was used in all tests.

The wooden fence frames use bamboo poles with a diameter of 0.08 – 0.10 m each, which is the mean diameter in the field (Albers et al. 2013; Anh et al. 2018; Schmitt et al. 2013). In this study, PVC piles with a diameter of 0.02 m were used as bamboo poles that scaled-down with a length scale of 5.0. The PVC piles are designed with a smooth surface and completely straight, leading to slightly less wave dissipation by these vertical poles. In the case of inner parts, the role of the PVC frames in wave damping could be neglected, but the design is conjectured to be closer to reality. Following the same construction as the field-frames, the frames were constructed from ten vertical piles over the flume width, producing an 8.7 cm distance between two piles (Figure 4a). The inner part contained inhomogeneous bamboo branches with a mean diameter of 0.004 m and consisted of the same material used for the steady flow experiments by Dao et al. (2020) (Figure 4b). Because brushwood fences were assembled from cylindrical PVC piles and bamboo sticks, the porosity could be calculated in a relatively straightforward fashion. The density of the inner parts was about 8705 piles/m^2 corresponding to the mentioned thicknesses above. The porosity was 0.90 for all thicknesses.

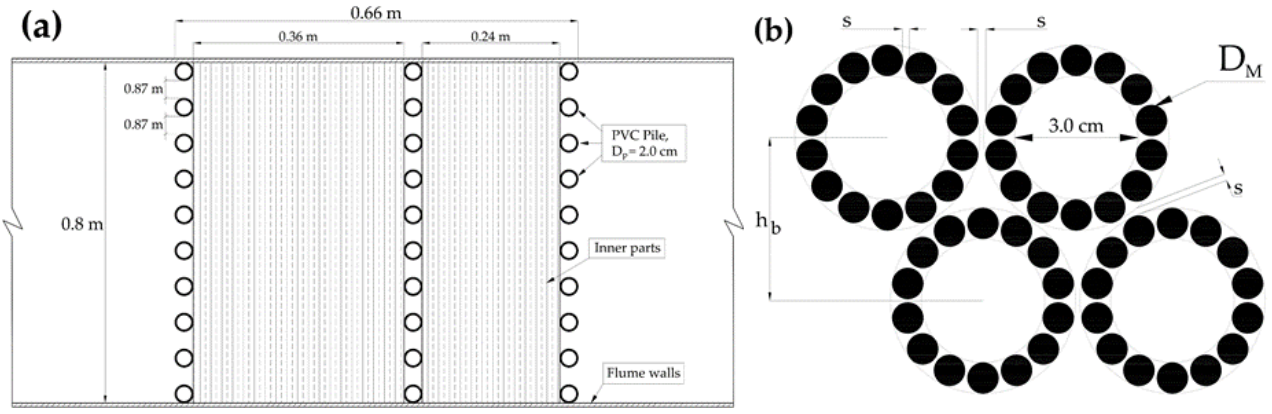

Figure 4: (a): The view from the top of a wooden fence. (b): In-homogenous arrangement of inner parts (Dao et al. 2020).

All Wave Gauges (WGs) had a sampling rate of 100 Hz. The measurements lasted at least 500 waves so that the gathering of representative statistical data could be collected. The error of WGs is given as 0.5% of the measuring range that was set as 0.1 m (Deltares, 2016). Two groups of gauges (WG1 to WG6) measured times series elevation used to extract incident and reflection waves in front of the wooden fence. The method of Zelt and Skjelbreia (1993) was applied to split the incident and the reflected wave signals. Then, the reflected and incident wave heights were calculated by the significant wave height, $H_{m0} = 4\sqrt{m_0}$ with m_0 is the zeroth-order moment of the water surface elevation. In particular, the incident wave signals of WGs1-3 were used as input boundaries of the numerical model. In contrast, wave elevations of WGs4-6 near the brushwood fence were used for calculating the incident and reflected waves (Figure 2). To calculate reflection and transmission coefficients following Equation (2) and (3), the incident ($H_{I,m0}$) and reflected wave heights ($H_{R,m0}$) were exacted from WGs4-6 signals at the location near the front face of the fence. It is noted that the method to extract incident and reflected wave heights are based on linear wave theory that can be applied for wave signals in front of the fence. However, transmitted wave heights are relatively small after damping by the fences leading to an increase of finite amplitude effects. As a result, an error in calculating incident and reflection for transmitted wave heights is inevitable (Zelt and Skjelbreia 1993). Therefore, the transmitted wave heights ($H_{T,m0}$) were calculated as the average of total wave heights measured by WGs7-9 signals behind the fence.

Based on the small-scale wave conditions in Table 2, tests were performed for three shallow water depths (d_m) that varied from 0.15 m to 0.25 m. It should be noted that the wooden fence was tested only in an emerged condition due to the limited dimensions of the wave flume. Peak periods (T_p) from 1.1 s to 2.7 s were used. For each water depth three fence thicknesses varying from 0.28 m to 0.66 m were applied (Table 4). The fence thicknesses were extended from a scaled value of B_m = 0.24 m (Table 2). This extension was aimed at testing the dependency of wave damping on fence thickness. For each combination of peak period, depth and fence thickness, three scaled significant wave heights ($H_{s,m}$) varying from 0.03 m to 0.075 m were imported in wave generator at deep water (Figure 2). As a result, there were a total of 27 tests performed in the wave flume. All tests were performed with irregular waves using the JONSWAP spectrum with peak enhancement factor γ = 3.3. Wave conditions were named from Val.01 to Val.09, as presented in Table 3.

Table 3: Characteristics of wave and wooden fence for the physical (Val cases) and numerical (Val and Sca cases) models.

Cases	Model scale				Prototype scale			
	B_m (m)	d_m(m)	$T_{p,m}$(s)	$H_{s,m}$(m) *	B_p (m)	d_p(m)	$T_{p,p}$(s)	$H_{s,p}$(m) *
Val.01	0.28	0.15	1.1	0.035; 0.055; 0.075	-	-	-	-
Val.02	0.28	0.20	1.2	0.030; 0.050; 0.070	-	-	-	-
Val.03	0.28	0.25	1.4	0.030; 0.050; 0.070	-	-	-	-
Val.04	0.40	0.15	1.3	0.030; 0.055; 0.070	-	-	-	-
Val.05	0.40	0.20	1.6	0.030; 0.050; 0.070	-	-	-	-
Val.06	0.40	0.25	1.8	0.030; 0.050; 0.070	-	-	-	-
Val.07	0.66	0.15	2.7	0.030; 0.045; 0.055	-	-	-	-
Val.08	0.66	0.20	2.4	0.030; 0.055; 0.070	-	-	-	-
Val.09	0.66	0.25	2.1	0.030; 0.055; 0.070	-	-	-	-
Sca.01	0.28; 0.40; 0.66; 0.92	0.15	2.1	0.06	1.4; 2.0; 3.3; 4.6	0.75	4.7	0.32
Sca.02	0.28; 0.40; 0.66; 0.92	0.25	2.1	0.11	1.4; 2.0; 3.3; 4.6	1.25	4.7	0.53
Sca.03	0.28; 0.40; 0.66; 0.92	0.30	2.1	0.14	1.4; 2.0; 3.3; 4.6	1.50	4.7	0.64
Sca.04	0.28; 0.40; 0.66; 0.92	0.35	2.1	0.15	1.4; 2.0; 3.3; 4.6	1.75	4.7	0.74
Sca.05	0.28; 0.40; 0.66; 0.92	0.45	2.1	0.19	1.4; 2.0; 3.3; 4.6	2.25	4.7	0.95
Sca.06	0.28; 0.40; 0.66; 0.92	0.55	2.1	0.23	1.4; 2.0; 3.3; 4.6	2.75	4.7	1.16
Sca.07	0.28; 0.40; 0.66; 0.92	0.15	2.4	0.06	1.4; 2.0; 3.3; 4.6	0.75	5.4	0.32
Sca.08	0.28; 0.40; 0.66; 0.92	0.25	2.4	0.11	1.4; 2.0; 3.3; 4.6	1.25	5.4	0.53
Sca.09	0.28; 0.40; 0.66; 0.92	0.30	2.4	0.14	1.4; 2.0; 3.3; 4.6	1.50	5.4	0.64
Sca.10	0.28; 0.40; 0.66; 0.92	0.35	2.4	0.15	1.4; 2.0; 3.3; 4.6	1.75	5.4	0.74
Sca.11	0.28; 0.40; 0.66; 0.92	0.45	2.4	0.19	1.4; 2.0; 3.3; 4.6	2.25	5.4	0.95
Sca.12	0.28; 0.40; 0.66; 0.92	0.55	2.4	0.23	1.4; 2.0; 3.3; 4.6	2.75	5.4	1.16

(*): Target wave height inputs at the offshore positions.

2.4 Numerical model

The SWASH model is applied to run the validation and scaling tests in this study. It is a time-domain model for simulating non-hydrostatic free-surface flow based on the non-linear shallow water equations, including the non-hydrostatic term (Zijlema et al. 2011). It can also accurately account for wave attenuation and wave breaking processes in the near-shore (Smit et al. 2013). In this study, the numerical model was set up based on the physical model, such that its results can exactly be compared to those of the physical model results. Next, the numerical models for scaling the simulations are presented, which are constructed similar to the physical model in the model-scale and the full-scale. Thus, the results can investigate the scale effects and wave-fence interactions.

The settings of the model- and full-scale runs are as follows. A spatial resolution (Δx) about $1/100$ of a peak wavelength (L_P) was applied as 0.01 m for all model calculations and 0.05 m for full-scale calculations resulting in 4000 grid points along with the profile, i.e., 40 m long for small-scale and 200 m for the large-scale model. The wave boundary for all tests was installed on the left side of the profile (Figure 2). For validation calculations, the wave boundary was set at x = 19.0 m (Figure 2), where the time series of incident surface elevation was imposed. The initial water level was set to zero. An initial time step of 0.001 seconds was employed for every simulation. Two vertical layers were applied for every numerical run to increase the accuracy of the validation runs.

Next, the validated wave model is used to quantify the scale effects in the 1:5 scale physical model and to determine the origin of scale effects. Wave conditions for scaling runs and their validation were presented in Table 3. For the validation runs, the same wave conditions were imposed as in the physical model tests, named Val.01 to Val.09. For scaling runs naming Sca.01 to Sca.12 in Table 3, each wave height was tested for one water depth corresponding to the ratio $H_{s,i}/d$ of roughly 0.42. Two wave periods were chosen as 2.1 and 2.4 s for small-scale tests corresponding to 4.7 and 5.4 s for full-scale simulations. For each wave condition, i.e., several peak wave periods, significant wave heights, and water depths, fence thicknesses were tested, as presented in Table 4. Besides the properties of the wooden fence for validation tests, the characteristics of the fence with a porosity of 0.81 used for the scaling, calculations are given.

Table 4: Characteristics of wooden fence used in numerical models.

Characteristics	Model scale		Full scale
Case	Val	Sca	Sca
Thickness, B (m)	0.28; 0.40; 0.66	0.28; 0.40; 0.66; 0.92	1.4; 2.0; 3.3; 4.6
Height, H_f (m)	0.30	0.30	1.50
Cylinder diameter, D (m)	0.004	0.004	0.02
Density, N_c (Cylinders/m^2)	8705	13077	603
Porosity, n (-)	0.90	0.81	0.81
Fence location (m)	28.0	28.0	140.0
Arrangement	Inhomogeneous	Staggered	Staggered
Test	Validation	Scaling	Scaling

The physical conditions that influence wave dissipation processes in this study include viscosity and bed friction. For model-scale tests, the vertical turbulence viscosity was set to 3.10^{-4} m^2/s, and Manning's roughness as bed friction coefficients were deployed as a default factor as 0.019 (m$^{-1/3}$s) (Zijlema et al. 2011). For the larger-scale runs, it is assumed that the flume was set with the same bed materials; therefore, bed friction should remain the same as at the small-scale tests. The inertia force was included with the added mass coefficient set for all tests as C_m = 1. It should be noted that only characteristics of the inner part were described in every simulation test. Further boundary conditions are described in Zijlema et al. (2011).

The main concern is the settings of wooden fences that are influenced by the drag coefficient in this study. In the version of the SWASH model (version 6.01), the vegetation model that can simulate wave reduction due to an array of stiff cylinders was applied to mimic wooden fences. The full description of the implementation of vegetation in SWASH, including horizontal cylinders, is given in Suzuki et al. (2019). In this model, the effects of the cylinder arrangement on the flow/waves are represented by the cylinder diameter, (and) the density of cylinders, and the bulk drag coefficient. The bulk drag coefficient for the present arrangement was obtained from experiments (e.g., Dao et al. 2020) at both the model- and the full-scale. The formulas of $\overline{C_D} - Re_n$ are presented in Table 1, and in this study, the Reynolds number is described as Re_n :

$$Re_n = \frac{U_{max} D}{n\nu} \tag{4}$$

where n is the porosity and U_{max} (m/s) is the maximum amplitude of the horizontal wave orbital velocity based on the linear wave theory for a wave with significant heights (H_{m0}).

The application of the $\overline{C_D} - Re_n$ relation in the wave simulations is not straightforward, as Re_n changes over the thickness and height of the fence. A representative bulk drag coefficient should be applied. The orbital wave velocity strongly depends on the wave height magnitude during the wave propagation progress. A reduction of wave height and decrease of wave velocity occur with the frontal contact along with the thickness. Indeed, Figure 5 illustrates wave heights (Figure 5a) and the maximum wave velocity at mid-water depth (Figure 5b) over the thickness of the wooden fence for the case with H_{m0} = 0.07 m; T_p = 2.1 s; d = 0.25 m; B = 0.66 m; and $\overline{C_D}$ = 4.2. It is shown that the wave height reduces along with the 0.66 m thickness from about 0.09 m to 0.04 m. As a result, the wave velocities and Re_n follow a similar trend. According to the measured relation between Re_n and $\overline{C_D}$ in prior experiments (Dao et al. 2020), the bulk drag coefficient increases with the decrease of wave velocity, and it reaches the highest value at the end of the wooden fence.

However, most wave dissipation occurs at the upstream side of the fence. Therefore, a location at the upstream side just inside the wooden fence (x = 28.05 m) was chosen to obtain the bulk drag coefficient. However, the $\overline{C_D}$ value cannot be achieved in a single run for validating the transmitted wave height, as the chosen value for $\overline{C_D}$ influences the velocity inside the fence. Thus, it is necessary to have an iterative computation to achieve an acceptable value of $\overline{C_D}$. With an initial value for $\overline{C_D}$ of one case, e.g., inhomogeneous and staggered case, one iteration was sufficient to obtain a converged value for K_T.

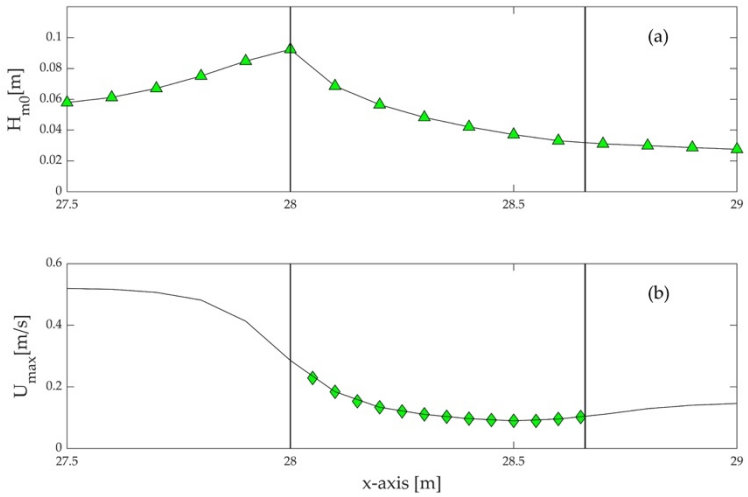

Figure 5: Wave heights (a) and maximum velocity (b) for the case with H_{m0} = 0.07 m; T_p = 2.1 s; d = 0.25 m; and B = 0.66 m.

After choosing a suitable location for the bulk drag coefficient, the relationship between the $\overline{C_D}$, that was applied in the last iteration run and the $\mathrm{Re_n}$, that was obtained with that $\overline{C_D}$, should follow the relation between the two parameters, as given in Table 1. Hence these combinations are plotted for all tested cases, including validation and scaling runs, in Figure 6 together with the relations from Table 1. The good correspondence shows that one iteration applied was sufficient. It should be noted that one wave condition shown in Table 3 can obtain one value of $\overline{C_D}$ even with the larger thickness fence. Therefore, a total of 27 values of $\overline{C_D}$ for validation runs and a total of 12 values of $\overline{C_D}$ for scaling runs are presented in Figure 6. All staggered cases can fit in one line due to the same porosity and configuration but different Reynolds numbers.

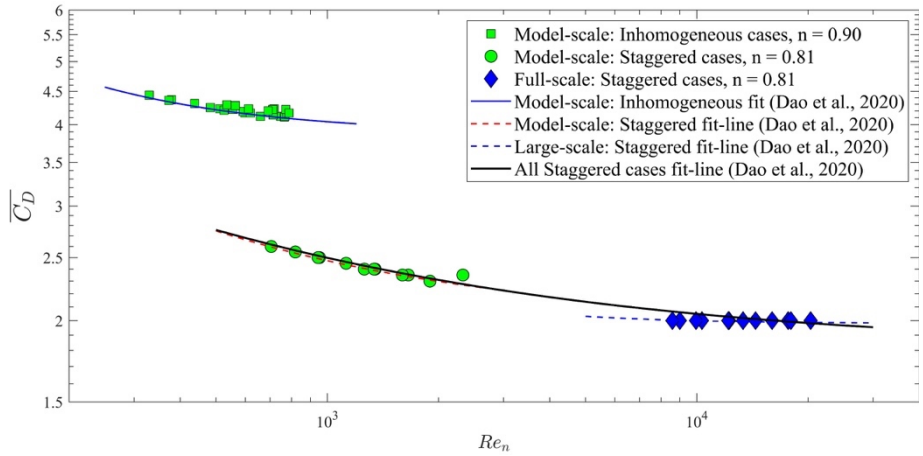

Figure 6: Drag coefficient and Reynolds number.

3 Results

In this section, the validation results are presented, in which the SWASH model is validated with the physical model results. The inspected parameters are the significant wave heights, and the surface elevation at wave gauges in front and behind wooden fences. Next, in Section 3.2, the interaction between waves and wooden fences is then presented, assessed by the reflection, dissipation, and transmission processes.

3.1 Validation results

First, the highest significant wave heights of case Val.01 to Val.09 (Table 3) are chosen to present wave transformation through wooden fences. The computed (blue line) and observed (green diamond) total significant wave heights are compared for the selected cases in Figure 7. Note that the observed wave heights at the measurement locations were within 10% of the target values. In general, the SWASH model results correspond well to the observed wave height variations. Especially for longer wave cases (Figure 7g, 7h, and 7i), the calculated node and anti-node standing wave pattern explain the wave height variation measured by the gauges in the physical model. Behind the fences, the SWASH results indicated that the measured significant wave height behind the fence is outside the standing wave pattern induced by the reflection from the slope at the end of the profile.

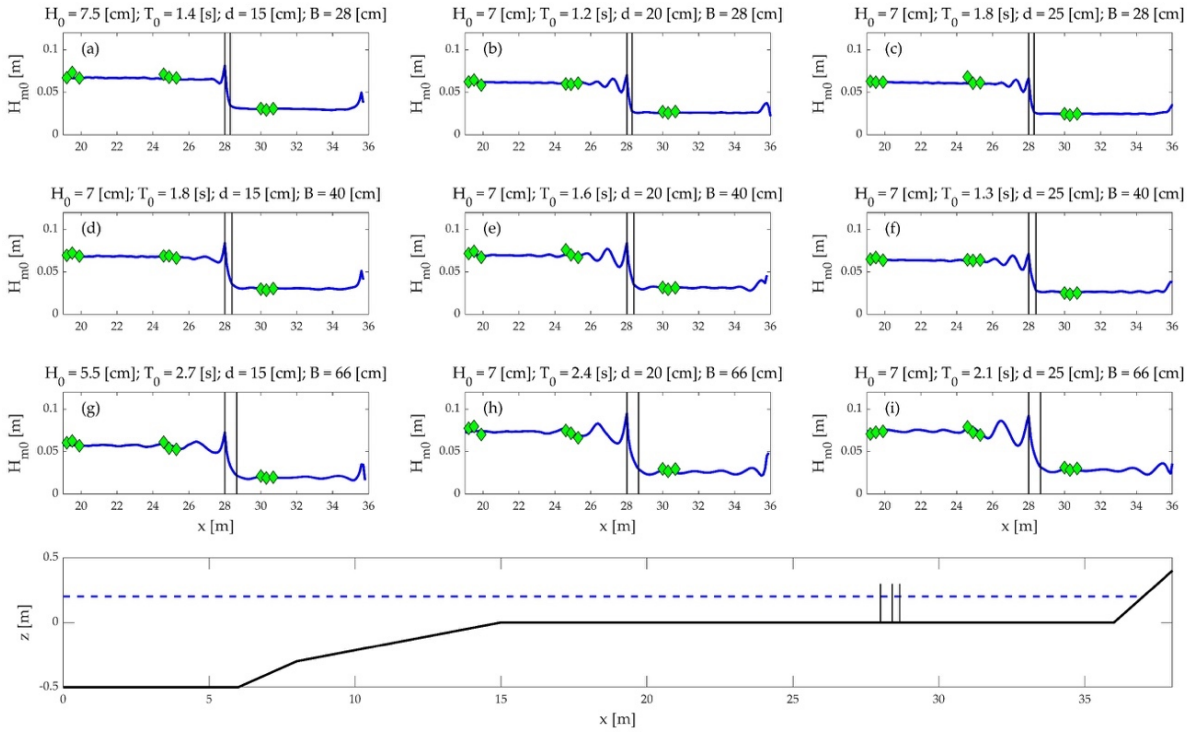

Figure 7: Comparing total significant wave heights between physical model (green diamond) and numerical model (blue line). Vertical lines at x = 28.0 m present for wooden fences.

Figure 8 compares the computed and recorded time series of the surface elevation for case Val.07 (Table 3) at three locations at the beginning of the foreshore (WG3, x = 19.9 m), in front of the wooden fence (WG6, x = 25.5 m), and behind the fence (WG7, x = 30.0 m). Generally, the comparison shows a good agreement between SWASH and the physical model results, especially at locations near the wooden fence. When the wave boundary for SWASH was located near 19.0 m, which is very close to the wave gauge 3, the surface signals were captured very well. At a location closer to the fence, gauge 6, the elevations between two models still agree well. The comparison at gauge 7 (between the wooden fence and dike) is not as good as those in front of the fence. The larger waves still seem to correspond well between experiment and simulation, but the phases of the higher frequency waves seem to be misrepresented.

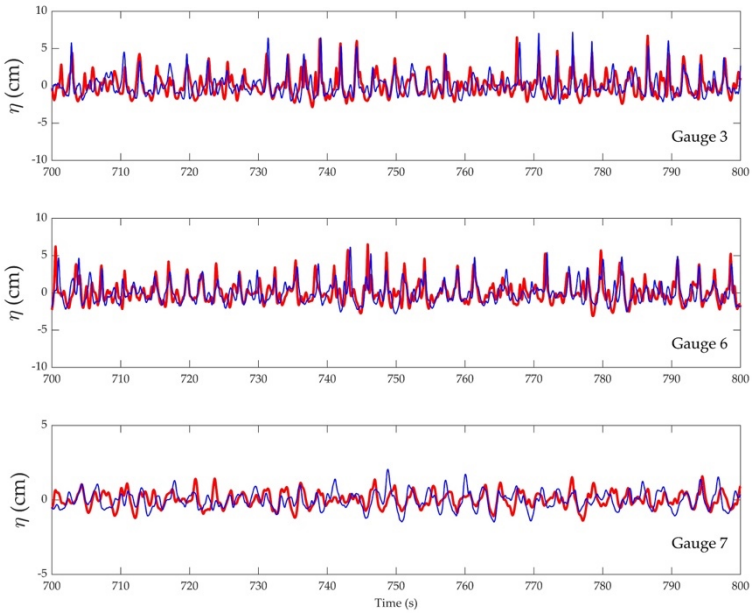

Figure 8: Comparison of water elevation between computation (thick red line) and observation (blue line): Top panel: at the beginning of the foreshore (WG3, x = 19.9 m); Middle panel: in front of the fence (WG6, x = 25.5 m); and Bottom panel: behind the fence (WG7, x = 30.0 m).

The corresponding wave spectral densities are derived by applying the Fast Fourier Transform (FFT) to water elevation data in Figure 8, as presented in Figure 9. A good agreement of total wave spectral densities between the computation (red dash line) and observation (solid blue line) for the mentioned cases is shown. The two spectra of the locations upstream of the fence show two peaks caused by the strong decrease in depth (Beji and Battjes 1993). The reproduction had a small mismatch at a peak at about 0.75 Hz and below 0.25 Hz at the beginning of the foreshore (WG3; x = 19.9 m, Figure 9a). At the location near the fence, WG6 (x = 25.5 m), the SWASH model reproduced the wave spectral density in comparison to the experimental one very well (Figure 9b). Behind the fence, SWASH might produce two peaks of the spectrum, while only one peak appeared from the measurement (Figure 9c). It is noted that in Figure 9c, the low-frequency spectrum was missed by the SWASH model compared to the observations. This mismatch might be due to the fact that the low-frequency waves are not being produced well after being filtered by the wooden fence. Moreover, the low frequencies (<0.25 Hz) are not well resolved due to the limited duration of both the computation and the experiment, and contain little energy. Hence it is difficult to draw firm conclusions about it.

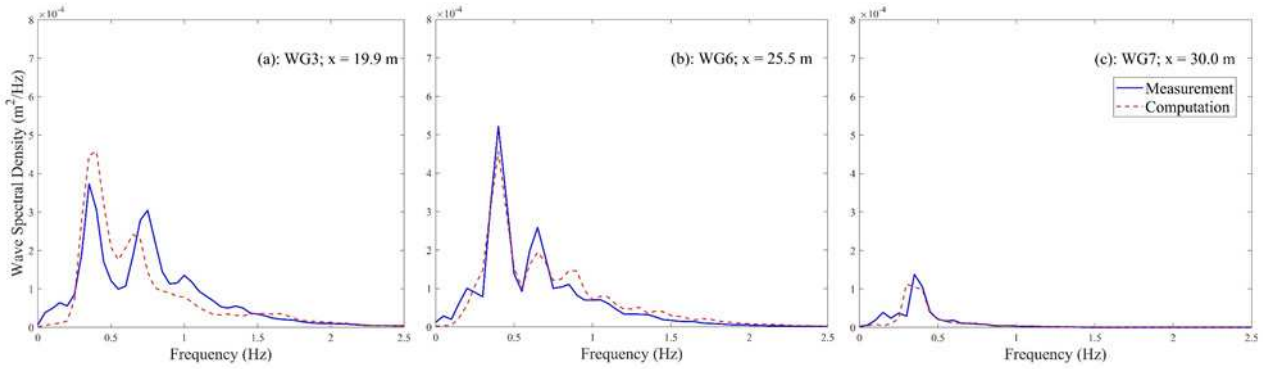

Figure 9: Comparison of wave spectral density between computation (red dash line) and observation (thick blue line) at the beginning of the foreshore (Gauge 3), in front of the fence (Gauge 5) and behind the fence (Gauge 7).

Furthermore, the predictive skill of SWASH was calculated applying the bias, and the scatter index SI, which is defined as:

$$\text{BIAS} = \frac{1}{N}\sum_{i=1}^{N}(\varphi_{comp}^{i} - \varphi_{obs}^{i}) \tag{5}$$

$$\text{SI} = \frac{\sqrt{\frac{1}{N}\sum_{i=1}^{N}(\varphi_{comp}^{i} - \varphi_{obs}^{i})^2}}{\frac{1}{N}\sum_{i=1}^{N}\varphi_{obs}^{i}} \tag{6}$$

where φ_{obs} and φ_{comp} are the corresponding values for the statistical wave parameters that were measured and computed by SWASH, respectively, and N is the total number of data points in the considered data set (Zijlema 2012).

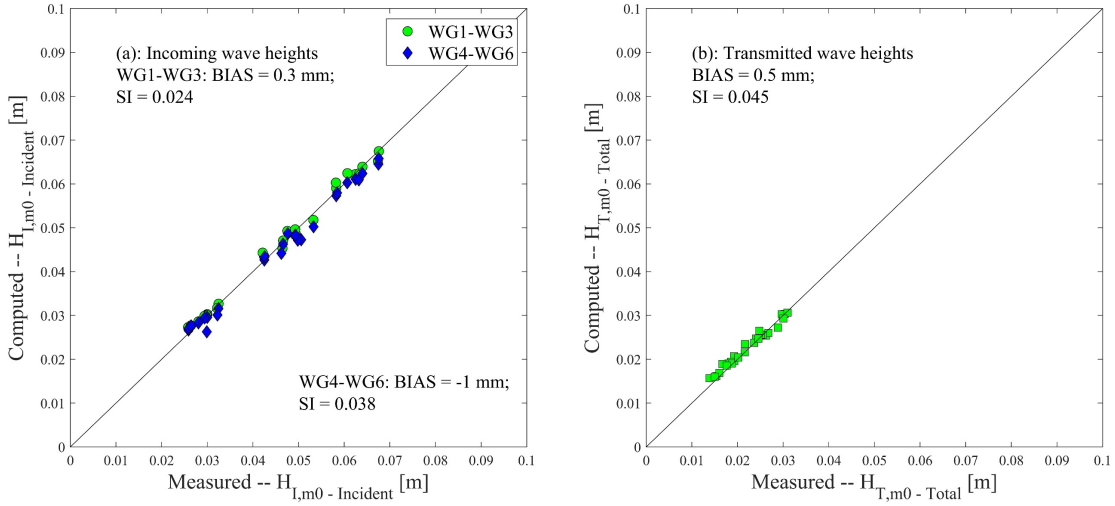

Figure 10: Comparison of wave heights between measurement and computation; (a): the incident wave heights $H_{I,m0}$; (b): the transmitted wave heights ($H_{T,m0}$).

Figure 10 indicates a good comparison of observation and computation of significant wave heights in front of and behind the wooden fence. In Figure 10a, the incident wave heights of WGs1-3 (green circle) and WGs4-6 (blue diamond) were generated with an acceptable level as the SI and BIAS are relatively low. For instance, the SI and BIAS of WGs1-3 are 2.4% and 0.3 mm, while these values of WGs4-6 are 3.8% and -1.0 mm, respectively. Figure 10a also shows that the reproduction of the significant incident wave heights from WGs4-6 was more accurate than WGs1-3. However, the errors are still relatively small compared to typical significant wave heights from 3.0 to 7.5 cm. It should be noted that there were no input values in the deep part of the computed domain. Thus, further calibration at the deep-water was not done. Comparison of the average significant wave heights of WGs7-9 for the measurement and computation are presented in Figure 10b. The average SI and BIAS of the transmitted significant wave heights are 4.5% and 0.5 mm.

3.2 Wave-fence interaction

The SWASH model has been validated with the physical model data using the bulk drag coefficient derived from separate experiments, as shown in the previous section. The result indicates that the numerical model can be used with confidence to simulate further scenarios for both model- and full-scale with the drag coefficients obtained from the separate experiments (Dao et al. 2020).

The interactions between waves and wooden fences are introduced in the previous sections and are expressed by the reflection (K_R), transmission (K_T), and dissipation (K_D) coefficients as defined in Equations (1), (2), and (3). To show the relationship between fence thickness and wave damping, these coefficients are plotted against relative fence thickness (B/H_I) for numerical results. The numerical results are used to explore the influence on the wave reducing properties of

two important parameters that can be altered in the design of the fence. These are the width of the fence and the characteristics of the brushwood branches.

As validated the numerical model in the previous section, the incoming and transmission waves are relatively matched resulting in a similarity of the expression of wave-fence interaction between the physical and numerical models. The relationship between wave-fence aspects of all full-fence cases Val.01 to Val.09 (Table 3) and the B/H_I is plotted in Figure 11. In the range of B/H_I from 4 to 23, a relatively small reflection in front of the wooden fence as K_R values around 0.4 (blue and green left-triangle), and a low wave transmission as K_T values range from 0.4 to 0.65 (blue and green hexagram) are indicated. Also, the efficiency of the wooden fence is therefore quantified by the dissipation coefficient, which increases from 0.8 to 0.9, occurs with the increase of B/H_I from 3 to 15, and keeps at about 0.9 until B/H_I increasing to 25 (blue and green diamond). The K_T value are about 0.4 to 0.55, with B/H_I from 4.0 to 15, which occurs for H_I/d within 0.25 to 0.30 (blue hexagram). Meanwhile, the higher K_T values, the lower wave reduction, are about 0.60 to 0.70 occurs with $H_I/d < 0.25$ (green hexagram). The reduction occurs due to small waves that are more damped by a wooden fence than larger waves. It is noticed that the wave reflection coefficient is less dependent on fence thickness. In both groups of H_I/d, the K_R values are about 0.3 to 0.4 with the increase of B/H_I (blue and green left-triangle). It should be noted that this transmission coefficient is based on the total wave height calculated from wave gauges downstream of the fence. Thereby, it is prone to some uncertainty discussed further in section Discussion.

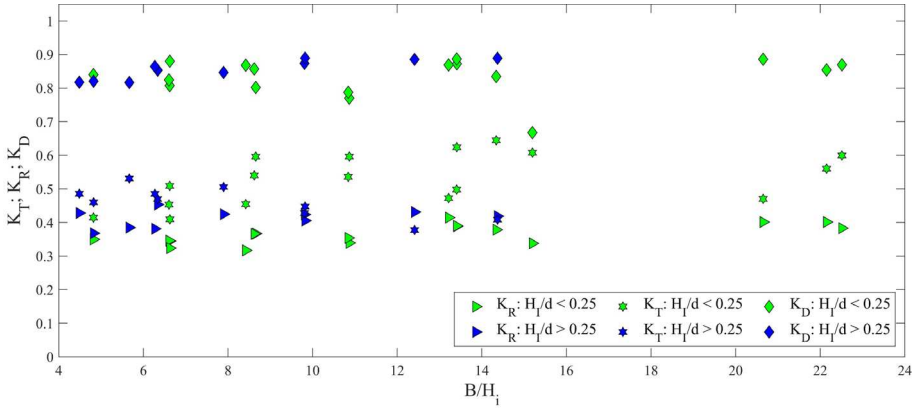

Figure 11: Plots of reflection, transmission, and dissipation coefficients against B/H_I for the physical model.

The relationships between B/H_I and reflection, transmission, and dissipation coefficient for all numerical runs, i.e., case Val.01 to Val.09 and Sca.01 to Sca.12 (see Table 3), are presented in Figure 12. For the case Sca.01 to Sca.12 with the same porosity ($n = 0.81$), the increases of these coefficients with the increase of B/H_I between the model-scale (green diamond) and the full-scale (blue circle) cases are quite similar. However, there is a small difference between the two scales, which is due to scale effects. This is explained in more details in the Discussion section. Particularly, the reflection and transmission of full-scale runs are slightly greater than the model-scale, as shown in Figures 12a and 12b, respectively. For instance, the K_R value of the full-scale model (blue circle) ranges from 0.40 to 0.55 while this value for the model-scale (green diamond) is from 0.35 to 0.45 in the same range of B/H_I from 1.0 to 15. The difference in K_T values between the two cases is about 0.05 within B/H_I from 1.0 to 5.0. In Figure 12c, the dissipation coefficient inside the wooden fence is interestingly matched for all inhomogeneous and staggered cases and increases from 0.7 to about 0.95 with an increase of B/H_I from 1.0 to 16.0. The results of these coefficients also indicate the dependency of wave reduction and reflection on fence thickness. The larger the thickness, the more wave damping.

However, data points of this case for relations K_R and $K_T - B/H_I$ are more scattered than the staggered cases for B/H_I from 8 to 16. It is due to these relations are in different group of H_I/d. Note that the H_I/d is larger than 0.40 for all scaling cases (Sca.01 to Sca.12) and is below 0.3 for all validation cases (Val.01 to Val.09). In Figure 12b, about 40% damping of small waves in $H_I/d < 0.25$ have occurred in inhomogeneous cases (Figure 11), while waves in $H_I/d > 0.25$ for inhomogeneous cases and $H_I/d > 0.42$ for staggered cases are damped with more than 50%. Within the same range of B/H_I from 8 to 16, the K_T values of inhomogeneous cases are significantly higher than staggered cases, e.g., about 0.5 compared to 0.2, respectively. In Figure 12c, the dissipation coefficients of all cases seem to be independent of porosity, as result points to converging within the range of B/H_I. The range of a transmission coefficient (K_T) from 0.2 to 0.7 is similar to the previous findings, i.e., Albers et al. (2013) and Schmitt et al. (2013). The reflection coefficients (K_T) from

0.2 to 0.4 only can be compared with the finding of Thieu Quang and Mai Trong (2020). The merged transmission coefficient in Figure 13b might indicate the dependency on H_I/d beside the B/H_I.

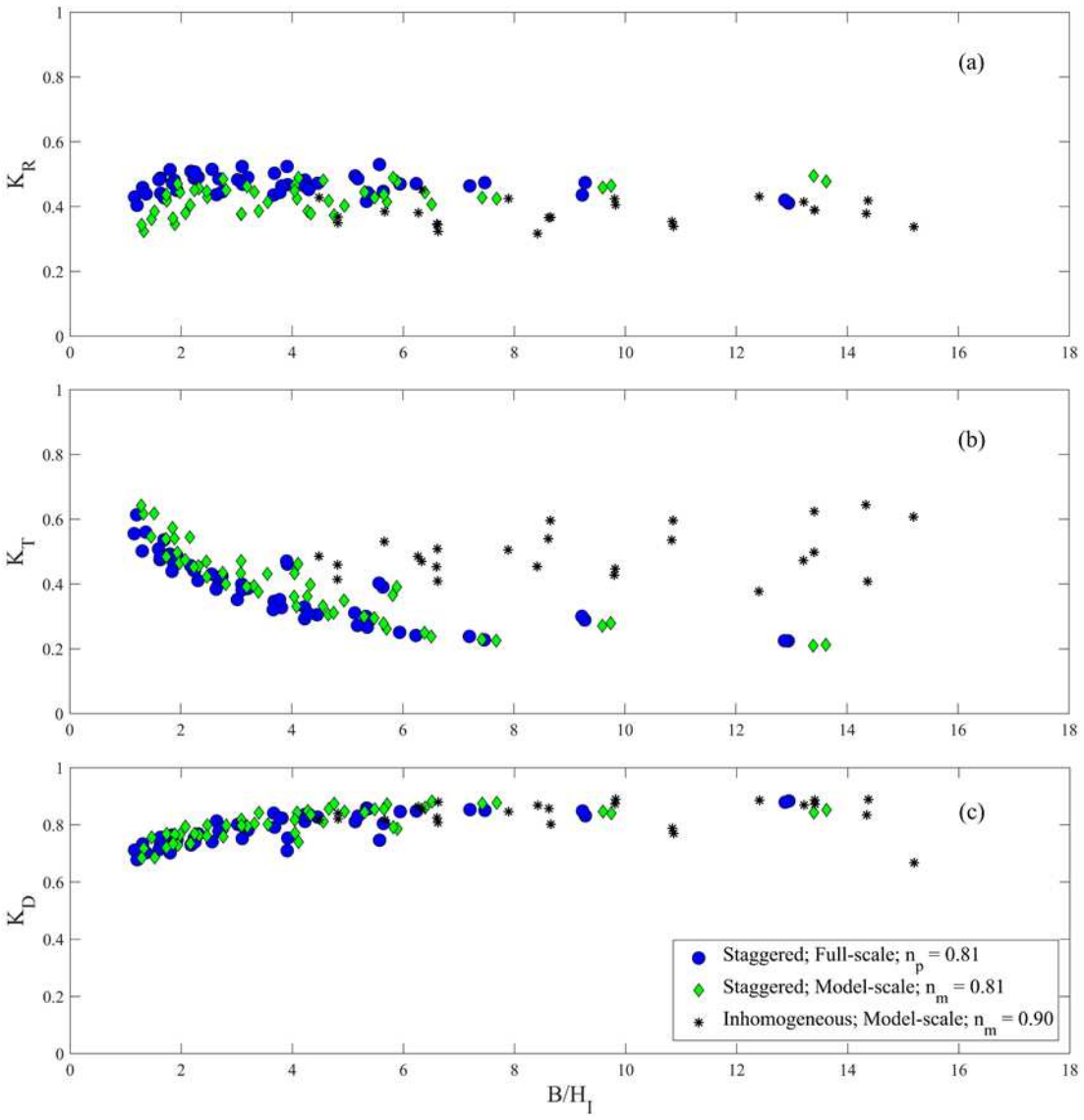

Figure 12: Relationship between reflection coefficients (a), transmission coefficient (b), and dissipation coefficient (c) and B/H_I.

4 Discussion

In the SWASH model, it is impossible to explicitly represent the configuration of branches (cylinders), usually characterized by an inhomogeneous arrangement in the field. The inhomogeneous parts have varying space between the branches, which also have different shapes and sizes. This configuration influences the drag forces corresponding to wave damping inside the structure (Dao et al. 2020). The $\overline{C_D}$ value is normally high in the laminar flow regime, Re_n < 1000, and lower in the turbulent flow, Re_n > 1000 (Dao et al. 2020). Thus, the amount of wave damping by the drag is parameterized by the bulk drag coefficient $\overline{C_D}$. This is a simple input parameter. Moreover, the cylinder diameter (D), and number of cylinders per area (N_c) should also be precisely defined, as in nature the branches gave a distribution of different sizes. Thus, with a careful definition of the characteristic value of the diameter, the drag coefficient is the main element for wave damping to parameterize the different arrangements of the cylinders of the inner parts.

The bulk drag coefficient is influenced by the scale effects of wooden fences when the laminar and turbulent effects occur for different sizes of materials and arrangements of a wooden fence. Under the laminar condition, normally $Re_n < 1000$, $\overline{C_D}$ values are high due to the high reduction of flow velocity at the upstream cylinders (Dao et al. 2020). If the model is scaled up, wave-flow conditions might become turbulent. In Figure 6, $\overline{C_D}$ is about 2.6 at $Re_n < 1200$ for small scale (red circles), while $\overline{C_D}$ is about 2.0 at $Re_n > 10^4$ for full scale (blue diamond). Due to the similar wave reduction, as was presented in Figure 14b, the scale effects were considered through the use of a Reynolds-dependent $\overline{C_D}$ value.

Scale effects come from aspects of resistance scaling which represent the resistance of fluid, for instance, the viscosity of the fluid and the bed friction. In theory, the influence of both viscosity and bed friction in the small-scale model is normally higher than that in the large-scale model. Therefore, by keeping the viscosity value the same in the full-scale model as in the laboratory condition in the physical model, its relative influence decreases if scaling up, as the momentum in the waves increases much more/significantly. The bed-friction value should be theoretically increased with a factor of $(N_L)^{1/6}$ and could be increased up to the maximum geometrical similarity ratio N_L (the length-scale) due to scaling up the model if including the viscosity of the fluid (Hughes 1993). Also, Hughes (1993) states that the effects of bed friction on wave propagation processes could play a major role if the N_L is much larger than 40. The unchanged viscosity might lead to the decrease of the bed friction for full-scale runs with a factor of $(N_L)^{1/6}$ which resulted in about 0.0145. In this study, the viscosity of fluid and bed friction were accounted for in all numerical simulations, which are based on laboratory conditions (see Numerical model description section).

In the numerical results shown in Figure 13, wave heights of full-scale are slightly greater than small-scales results, particularly in the shallowest water depth (Figure 13a and 13b). This difference indicates a dependency of small-scale wave dissipation on bed friction rather than full-scale waves. Thus, the scale effects might be greater than the bed friction effects, for the shallowest water depth. It is noticed that the difference between the two scales is narrowed when water depths increase for case Sca.12 (d_m = 0.55 m and d_p = 2.75 m), as shown in Figure 13c and Figure 13d, respectively. The small-scale wave dissipation might depend more on bottom friction than the larger-scale waves at a shallow water depth. Furthermore, the wave dissipation might then also be less affected by the bottom friction as the dispersion rate of the wave orbital at water depths increases. The scale effects of bulk drag coefficients on transmitted wave heights can also be seen in Figure 13b, and 13d. As can be seen, the dissipation rates inside the wooden fence for case Sca.07 (Figure 13b) are not the same, which is caused by the difference of the bulk coefficient due to added laminar friction. Note that the low magnitude model-scale wave condition ($T_{p,m}$ = 2.4 s, $H_{s,m}$ = 0.06 m, and d_m = 0.15 m) of case Sca.07 creates a more laminar flow condition leading to a higher bulk drag coefficient (Dao et al. 2020). Thus, for this case, the friction from the bottom and laminar friction inside the wooden fences are most influenced by scale effects. Conversely, the scale effects of bottom friction on wave heights in front of the fences are less important for case Sca.12 (Figure 13d), which have a higher wave height and Reynolds numbers. In contrast, the more constant $\overline{C_D}$ value, generated by turbulent friction for the larger wave conditions, results in a lower wave dissipation. The results might indicate that the bottom friction and viscosity effects can be neglected when incoming wave heights and water depth are larger than 0.15 m and 0.3 m, respectively.

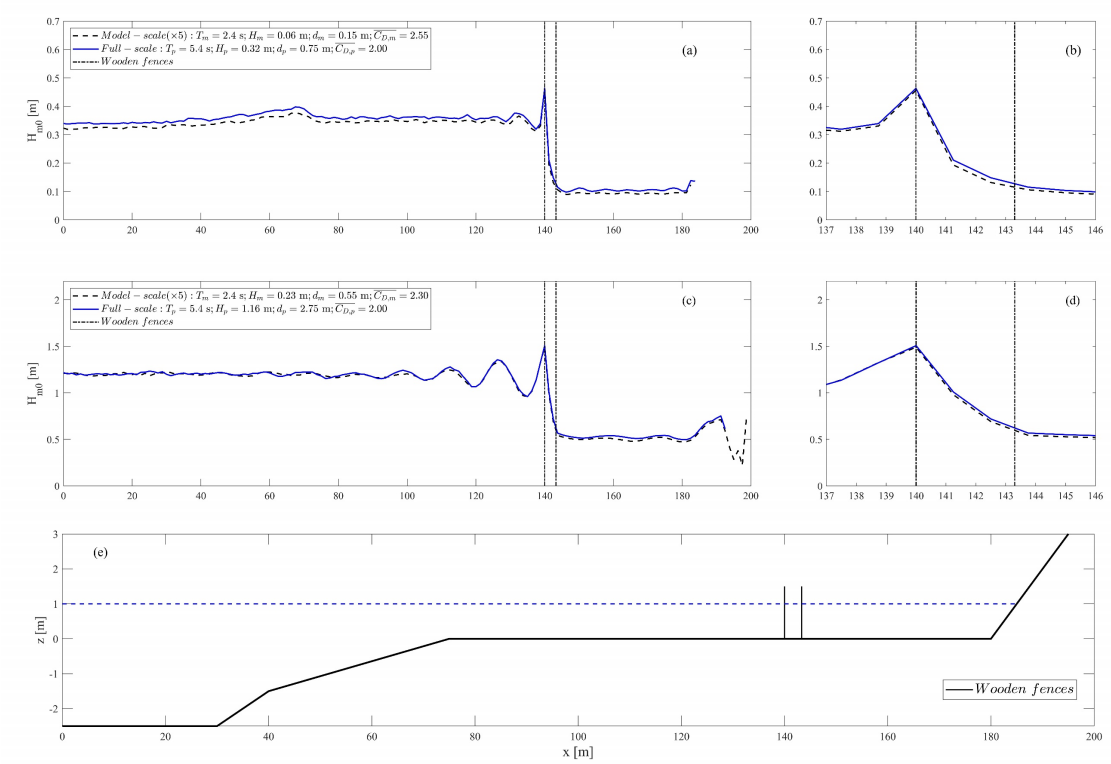

Figure 13: Wave transformation through wooden fences (dash-dot line) for upscaled small-scale (dash line) and full-scale cases (blue line). Waves transform in the entire domain and inside the wooden fence for case Sca.07 (a, b), and case Sca.12 (c, d). The foreshore bathymetry is given as reference (e).

To investigate further the scale effects, the power regressions of two scales between K_R, K_T, and K_D and B/H_I of all staggered cases (Sca.01 to Sca.12, Table 3) with the best fits $R^2 > 0.80$ are plotted in Figure 14. As can be seen, a small difference in K_T between two cases with 0.81 porosity for model-scale (black line) and full-scale (blue line). An average 5% difference of K_T for the model-scale is higher than the full-scale cases at $B/H_I < 5.5$. However, this difference becomes smaller and consequently merges at $B/H_I > 10$. This result indicates the scale effect might occur for the larger wave height compared to a fence thickness when models are scaled up. If the scale factor is larger, this difference should be greater.

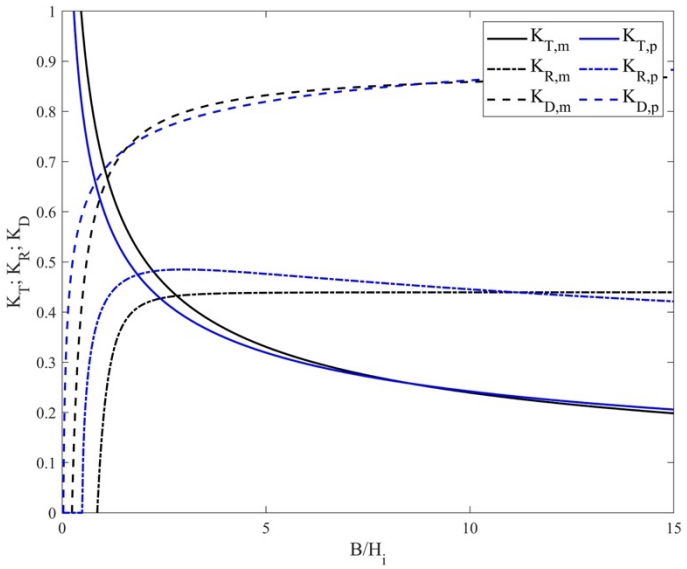

Figure 14: Comparison of power fits between scaling cases.

It is shown that the SWASH model is a suitable tool to evaluate the optimal configuration for the fence design. It could be used to show the function of the fence in more realistic 2D and 3D bathymetries. Moreover, it is indicated that the small-scale modelling can be applied for design with limited scale effects if wave height and small-scale branch diameter are larger than 0.15 m and 0.004 m, respectively. The results also highlight the more efficient wave damping when applying an inhomogeneous arrangement of brushwood inner parts. Additionally, as the low frequency energy is slow, it has lower velocities and Reynolds' numbers. Therefore, the low frequency wave energy could be subject to scale effects due to extra (viscous) damping.

The appearance of a dike at the end of the profile (see Figure 2) can generate wave reflection in front of it. After a wooden fence damps the incoming waves, the transmitted wave heights can be calculated as the incident- and total-transmitted heights. However, as mentioned in the Physical model section, the method used to calculate incident and reflection for transmitted waves is unavailable due to limited wave gauges. In the physical model, the unavailability of data leads to uncertainty if choosing the only incident transmitted wave heights to calculate the transmission coefficient. In the numerical model, this issue can be solved by replacing the dike at the end of the profile with a non-reflective boundary to achieve an appropriate transmission coefficient. From an engineering perspective, even though the incident wave heights might be a correct way to calculate transmission coefficient, the configuration including a dike is more realistic.

5 Conclusion

In this study, the interaction between wooden fences and waves is investigated by applying the numerical model SWASH. The SWASH model used for simulating wave damping by wooden fences was firstly validated by using the bulk drag coefficient obtained from Dao et al. (2020) and the data from physical model results. The wooden fence used in the physical model contains horizontal inhomogeneous brushwood that also used in experiments by Dao et al. (2020). The needed wave data for validation, including incoming and transmission wave heights, was also obtained. Additionally, the physical results indicated the dominant influence of the inner parts and the negligible influence of the frames on wave reduction. The validation results had a good agreement with the physical results without any model tuning or calibration, indicating the bulk drag coefficient was the key element to simulate wave reduction by the wooden fence in the SWASH model.

The scaling calculations were run with the characteristics of the inner part of the wooden fence, represented by the bulk drag coefficient, directly obtained from Dao et al. (2020), for an identical arrangement measured at the two scales. Even though the Froude scale factor of 5.0 used in this study is significantly smaller than the literature suggested (Hughes, 1993), the scale effect has still occurred. Both reflection and transmission of small-scale waves are about 10% lower than a full-scale wave in which the difference between two scales is about 0.05 with $B/H_I < 5.5$. The scale effects are largest for the thin fence thickness and small waves. The water depth (d_m) and incoming wave heights ($H_{s,m}$) should be larger 0.3 m and 0.15 m, respectively, to have the negligible effects of bed friction and viscosity effects inside the fence even though the model effect might still have occurred.

The further scaling simulations together with the initial results of validation processes demonstrate the larger the wave, the more the damping that presented by the dimensionless parameter, H_I/d and B/H_I. This is proven by the fact that the range of about more than 70% of incoming waves are damped for cases with $H_I/d > 0.25$ for inhomogeneous fences and $H_I/d > 0.4$ for staggered fences. Moreover, the transmission coefficient is dependent on the B/H_I indicated by the reduction of this coefficient with the increase of B/H_I for all cases with $H_I/d > 0.4$. For all scaling results, both K_T and K_R from the numerical model are also in the same range as observed in the field.

Even though the bulk drag coefficient is the most important input parameter for the numerical model, there are still several uncertainties in choosing the acceptable value for the field's wooden fence. For example, the highly irregular shape of bamboo branches and their arrangements in the field (Figure 1) might lead to a higher value of the bulk drag coefficient for further numerical application. For this part, future research needs to continue and contribute to this study of importance to the healthy and sustained environment of mangroves.

Acknowledgements

The first author (H.T. Dao) is grateful for being supported by Delft University of Technology, the Netherlands; the Ministry of Education and Training, Vietnam International Education Cooperation Department, Vietnam; Hanoi University of Natural Resources and Environments, Hanoi, Vietnam; the National Project (project code: KC.09.21/16–20) and the ministerial projects (project code: B2020-XDA-02). We acknowledge Mariette van Tilburg for reviewing and editing the manuscript. We also thank Sander De Vree, Jaap van Duin, Frank Kalkman, and Arno Doorn for assisting with construction and measurement in the laboratory.

Author contributions (CRediT)

HTD: Conceptualization, Data curation, Formal Analysis, Investigation, Methodology, Writing – original draft, and Writing – review & Editing. BH: Conceptualization, Methodology, Supervision, and Writing – review. TS: Supervision, and Writing – review. MS: Supervision, and Writing – review. TM: Writing – review. LXT: Writing – review.

References

Albers, T.; San, D. C.; Schmitt, K. (2013): Shoreline Management Guidelines: Coastal Protection in the Lower Mekong Delta. In: Deutsche Gesellschaft für Internationale Zusammenarbeit (GiZ) GmbH Management of Natural Resources in the Coastal Zone of Soc Trang Province, 1, S. 1–124.

Anderson, M. E.; Smith, J. M. (2014): Wave attenuation by flexible, idealized salt marsh vegetation. In: Coastal Engineering (Elsevier), 83, S. 82–92.

Anh, N.; Mai, T.; Mai, C. (2018): Wave reduction by a bammboo fence. In International Symposium on Lowland Technology, Hanoi, Vietnam, September 2018

Beji, S.; Battjes, J. A. (1993): Experimental investigation of wave propagation over a bar. In: Coastal Engineering (Elsevier), 19(1–2), S. 151–162.

Buckley, M. L.; Lowe, R. J.; Hansen, J. E.; Van Dongeren, A. R. (2015): Dynamics of wave setup over a steeply sloping fringing reef. In: Journal of Physical Oceanography, 45(12), S. 3005–3023.

Chen, H.; Ni, Y.; Li, Y.; Liu, F.; Ou, S.; Su, M.; Peng, Y.; Hu, Z.; Uijttewaal, W.; Suzuki, T. (2018): Deriving vegetation drag coefficients in combined wave-current flows by calibration and direct measurement methods. In: Advances in water resources (Elsevier), 122, S. 217–227.

Van Cuong, C.; Brown, S.; To, H. H.; Hockings, M. (2015): Using Melaleuca fences as soft coastal engineering for mangrove restoration in Kien Giang, Vietnam. In: Ecological Engineering (Elsevier), 81, S. 256–265.

Dalrymple, R. A.; Kirby, J. T.; Hwang, P. A. (1984): Wave diffraction due to areas of energy dissipation. In: Journal of Waterway, Port, Coastal, and Ocean Engineering, In: American Society of Civil Engineers, 110(1), S. 67–79.

Dao, H. T.; Hofland, B.; Stive, M. J. F.; Mai, T. (2020): Experimental Assessment of the Flow Resistance of Coastal Wooden Fences. In: Water.

Dao, T.; Stive, M. J. F.; Hofland, B.; Mai, T. (2018): Wave Damping due to Wooden Fences along Mangrove Coasts. In: Journal of Coastal Research, 34(6), S. 1317–1327.

Deltares: Wave height meter (2016). In Deltares. Available in: https://www.deltares.nl/app/uploads/2016/04/Wave-height-meter.pdf.

Gagliano, S. M.; McIntire, W. G. (1968): Reports on the Mekong River Delta. In: Lousiana State Univ. Baton Rouge Coastal Studies Inst.

Gijón Mancheño, A.; Tas, S. A. J.; Herman, P. M. J.; Reniers, A.; Uijttewaal, W. S. J.; Winterwerp, J. C. (2017): Wave attenuation by brushwood dams in a mud-mangrove coast. In: INTERCOH 2017.

Heller, V. (2011): Scale effects in physical hydraulic engineering models. In: Journal of Hydraulic Research (Taylor & Francis), 49(3), S. 293–306.

Hoang, V. H.; Nguyen, H. N. (2006): Result on study of wave field on Dong Nai, Sai Gon estuaries and suggestion of sea bank and river mouth protection methods. In: Vietnam-Japan Estuary Workshop in collaboration between Tohoku University and Water Resources University, S. 140–150.

Hu, Z.; Suzuki, T.; Zitman, T.; Uittewaal, W.; Stive, M. (2014): Laboratory study on wave dissipation by vegetation in combined current–wave flow. In: Coastal Engineering (Elsevier), 88, S. 131–142.

Hughes, S. A. (1993): Physical models and laboratory techniques in coastal engineering. In: World Scientific.

Keulegan, G. H. (1958): Forces on cylinders and plates in an oscillating fluid. In: J. Research of the National Bureau of Standards Research Paper, 2857, S. 423–440.

Mai, S.; von Lieberman, N.; Zimmermann, C. (1999): Interaction of foreland structures with waves. In: XXVIII IAHR congress, Graz.

Mendez, F. J.; Losada, I. J. (2004): An empirical model to estimate the propagation of random breaking and nonbreaking waves over vegetation fields. In: Coastal Engineering (Elsevier), 51(2), S. 103–118.

Morison, J. R.; Johnson, J. W.; Schaaf, S. A. (1950): The Force Exerted by Surface Waves on Piles. In: Society of Petroleum Engineers.

Nguyen, V. L.; Ta, T. K. O.; Tateishi, M. (2000): Late Holocene depositional environments and coastal evolution of the Mekong River Delta, Southern Vietnam. In: Journal of Asian Earth Sciences (Elsevier), 18(4), S. 427–439.

Novák, P.; Čábelka, J. (1981): Models in hydraulic engineering: Physical principles and design applications. In: Pitman Publishing.

Ozeren, Y.; Wren, D. G.; Wu, W. (2013): Experimental investigation of wave attenuation through model and live vegetation. In: Journal of Waterway, Port, Coastal, and Ocean Engineering, In: American Society of Civil Engineers, 140(5), S. 4014019.

Phan, K. L.; Stive, M. J. F.; Zijlema, M.; Truong, H. S.; Aarninkhof, S. G. J. (2019): The effects of wave non-linearity on wave attenuation by vegetation. In: Coastal Engineering (Elsevier), 147, S. 63–74.

Phan, L. K.; van Thiel de Vries, J. S. M.; Stive, M. J. F. (2014): Coastal Mangrove Squeeze in the Mekong Delta. In: Journal of Coastal Research, In: Coastal Education and Research Foundation, S. 233–243.

Reis, R. A.; Pires-Silva, A. A.; Fortes, C. J.; Suzuki, T. (2020): Experiences with SWASH on modelling wave propagation over vegetation. In: Journal of Integrated Coastal Zone Management; Vol 20 No 2 (2020): Coastal Zones Volume I.

Roelvink, J. A.; Stive, M. J. F. (1989): Bar-generating cross-shore flow mechanisms on a beach. In: Journal of Geophysical Research: Oceans, In: Wiley Online Library, 94(C4), S. 4785–4800.

Sayah, S.; Schleiss, A. (2006): Efficiency of brushwood fences in shore protection against wind-wave induced erosion. In: EPFL-LCH.

Schmitt, K.; Albers, T. (2014): Area coastal protection and the use of bamboo breakwaters in the Mekong Delta. In: Coastal Disasters and Climate Change in Vietnam (Elsevier), S. 107–132.

Schmitt, K.; Albers, T.; Pham, T. T.; Dinh, S. C. (2013): Site-specific and integrated adaptation to climate change in the coastal mangrove zone of Soc Trang Province, Viet Nam. In: Journal of Coastal Conservation, 17(3), S. 545–558.

Smit, P.; Zijlema, M.; Stelling, G. (2013): Depth-induced wave breaking in a non-hydrostatic, near-shore wave model. In: Coastal Engineering (Elsevier), 76, S. 1–16.

Suzuki, T.; Hu, Z.; Kumada, K.; Phan, L. K.; Zijlema, M. (2019): Non-hydrostatic modeling of drag, inertia and porous effects in wave propagation over dense vegetation fields. In: Coastal Engineering (Elsevier), 149, S. 49–64.

Suzuki, T.; Zijlema, M.; Burger, B.; Meijer, M. C.; Narayan, S. (2012): Wave dissipation by vegetation with layer schematization in SWAN. In: Coastal Engineering (Elsevier), 59(1), S. 64–71.

Ta, T. K. O.; Nguyen, V. L.; Tateishi, M.; Kobayashi, I.; Saito, Y.; Nakamura, T. (2002): Sediment facies and Late Holocene progradation of the Mekong River Delta in Bentre Province, southern Vietnam: an example of evolution from a tide-dominated to a tide-and wave-dominated delta. In: Sedimentary Geology (Elsevier), 152(3), S. 313–325.

Tanino, Y.; Nepf, H. M. (2008): Laboratory investigation of mean drag in a random array of rigid, emergent cylinders. In: Journal of Hydraulic Engineering (American Society of Civil Engineers), 134(1), S. 34–41.

Thieu Quang, T.; Mai Trong, L. (2020): Monsoon wave transmission at bamboo fences protecting mangroves in the lower mekong delta. In: Applied Ocean Research, 101, S. 102259.

Thornton, E. B.; Calhoun, R. J. (1972): Spectral resolution of breakwater reflected waves. In: Journal of Waterways, Harbors & Coast Eng Div, 98(9318 Proceeding).

Tsai, C.-P.; Chen, H.-B.; Hwung, H.-H.; Huang, M.-J. (2005): Examination of empirical formulas for wave shoaling and breaking on steep slopes. In: Ocean Engineering (Elsevier), 32(3–4), S. 469–483.

Del Valle, A.; Eriksson, M.; Ishizawa, O. A.; Miranda, J. J. (2020): Mangroves protect coastal economic activity from hurricanes. In: Proceedings of the National Academy of Sciences (National Acad Sciences), 117(1), S. 265–270.

Wolanski, E.; Huan, N. N.; Nhan, N. H.; Thuy, N. N. (1996): Fine-sediment dynamics in the Mekong River estuary, Vietnam. In: Estuarine, Coastal and Shelf Science (Academic Press), 43(5), S. 565–582.

Zelt, J. A.; Skjelbreia, J. E. (1993): Estimating incident and reflected wave fields using an arbitrary number of wave gauges. In: Coastal Engineering 1992, S. 777–789.

Zijlema, M. (2012): Modelling wave transformation across a fringing reef using SWASH. In: ICCE 2012: Proceedings of the 33rd International Conference on Coastal Engineering, Santander, Spain, 1-6 July 2012, In: Coastal Engineering Research Council.

Zijlema, M.; Stelling, G.; Smit, P. (2011): SWASH: An operational public domain code for simulating wave fields and rapidly varied flows in coastal waters. In: Coastal Engineering (Elsevier), 58(10), S. 992–1012.